A hybrid finite element/finite difference time domain electromagnetic approach to the analysis of high frequency FET devices

INTERNATIONAL JOURNAL OF NUMERICAL MODELLING: ELECTRONIC NETWORKS, DEVICES AND FIELDS
Int. J. Numer. Model. 2000; **13**:289–300

A hybrid finite element/finite difference time domain electromagnetic approach to the analysis of high-frequency FET devices

A. Monorchio[1], A. Cidronali[2], G. Manara[1] and G. Pelosi[2,*]

[1] *Department of Information Engineering, University of Pisa, via Diotisalvi 2, I-56126 Pisa, Italy*
[2] *Department of Electronic Engineering, University of Florence, via C. Lombroso 6/17, I-50134 Florence, Italy*

SUMMARY

A comprehensive simulation procedure is presented for describing the behaviour of high-frequency field effect transistors (FETs). It combines a circuit model of the intrinsic part of the device with a hybrid finite elements/finite differences (FE/FD) technique directly implemented in time domain (TD). This latter method allows us to efficiently reconstruct the actual electromagnetic field distribution in the different regions of the FET. Indeed, FD are suitable to describe non-linear effects in the active part of the device, while finite elements efficiently account for material inhomogeneities and complex geometrical shapes. The resulting simulation model includes both electromagnetic wave propagation and charge transport phenomena. Copyright © 2000 John Wiley & Sons, Ltd.

1. INTRODUCTION

The increasing number of applications in the field of millimeter and microwave integrated components (MMIC) has recently produced a considerable effort in the development of computer models for the design of high-frequency active electron devices. In this context, suitable numerical techniques are needed to implement general computer-aided design (CAD) tools for an efficient and accurate simulation of transistors as well as monolithic and hybrid integrated components (ICs). Generally speaking, high-frequency electron devices have been conventionally simulated by separately considering electromagnetic wave propagation and charge transport phenomena. First attempts to fully consider the coupling between these two aspects of the device physics have been recently proposed in the literature [1–3]. The finite difference-time domain (FD-TD) technique can suitably account for the non-linear behaviour of the device active region; however, since a proper description of the charge transport phenomenon usually requires the adoption of a nanometer-order space discretization, conventional space meshing rapidly leads to a high number of unknowns, considerably increasing computational efforts. Moreover, an accurate description of the device geometry may require a greater flexibility than that offered by FD-TD.

* Correspondence to: G. Pelosi, Department of Electronic Engineering, University of Florence, via C. Lombroso 6/17, I-50134 Florence, Italy.

Contract/grant sponsor: Italian-Spanish Integrated Action; contract/grant number: HI1966-0022
Contract/grant sponsor: Italian Research Council MADESS II; contract/grant number: CU99.00113.48

A hybrid finite element/finite difference time domain (FE/FD-TD) procedure is applied in this work, allowing us to overcome the typical restrictions of an approach based on the only FD-TD method [4–7]. By analysing the device physics it is seen that two separate regions can be identified where the internal device dynamics is governed by mechanisms of different kind. The first region represents the active area of the device, where charge transport phenomena occur, and will be referred to as the *intrinsic* device. The other region provides interconnections between the *intrinsic* device and each external terminal, and will be referred to as the *extrinsic* device. The presence of dielectric stratifications must be accounted for in modelling this second zone. The *intrinsic* part of the device is described by the FD-TD method, which is applied in combination with a circuit model describing charge transport effects. These latter effects are introduced in the electromagnetic simulation through suitable electric current distributions, providing equivalent sources for the determination of the fields in the whole device. In particular, the *extrinsic* region is analysed by resorting to a hybrid FE/FD-TD technique which results in a more flexible tool from both geometrical modelling accuracy and computational efficiency points of view. It is worth noting that the interaction between electron transport and electromagnetic fields has been analysed in the transverse section of the FET (two-dimensional case). Consequently, the work is not directly applicable to real configurations. However, the paper is basically aimed to show that this more flexible technique is viable for such kind of problems; the extension to a three-dimensional case will be object of future work.

The paper has been organized as follows. The global simulation procedure is described in Section 2. Some features of the hybrid electromagnetic method adopted are given in Section 3. Then, numerical results are presented in Section 4, in order to demonstrate the effectiveness of the simulation technique. Finally, some concluding remarks are drawn in Section 5.

2. ELECTRON DEVICE MODEL FORMULATION

This section describes the global simulation scheme of the whole electronic device, focusing on the interconnection between the model of the active region, namely the *intrinsic* part, and that of the *extrinsic* part of the transistor, which accounts for any passive effect due to the electrodes and dielectric layers. Although a more general description of the problem would require a three-dimensional approach, we note that several real structures exhibit uniform characteristics both in geometry and material constitution with respect to a specific axis. This allows us to model the device in its cross-section, then extending the obtained results to three dimensions by simply exploiting uniformity. The cross-section view of a typical high-frequency FET is shown in Figure 1. A conventional AlGaAs\GaAs HEMT will be considered in the following.

The FET active region is analysed by using the FD-TD approach due to its inherent simplicity in handling non-linear equations. More specifically, the FD-TD electromagnetic simulation scheme is interfaced with a circuit model of the active region through the conduction density current $\mathbf{J}(\mathbf{r}, t)$ arising in Maxwell equations, i.e.

$$\nabla \times \mathbf{H}(\mathbf{r}, t) = \varepsilon(\mathbf{r}) \frac{\partial \mathbf{E}(\mathbf{r}, t)}{\partial \mathbf{t}} + \mathbf{J}(\mathbf{r}, t) \tag{1}$$

where $\mathbf{H}(\mathbf{r}, t)$ and $\mathbf{E}(\mathbf{r}, t)$ are the magnetic and the electric fields, respectively, and $\varepsilon(\mathbf{r})$ is the dielectric permittivity of the medium. According to the electronic model, the current $\mathbf{J}(\mathbf{r}, t)$ is

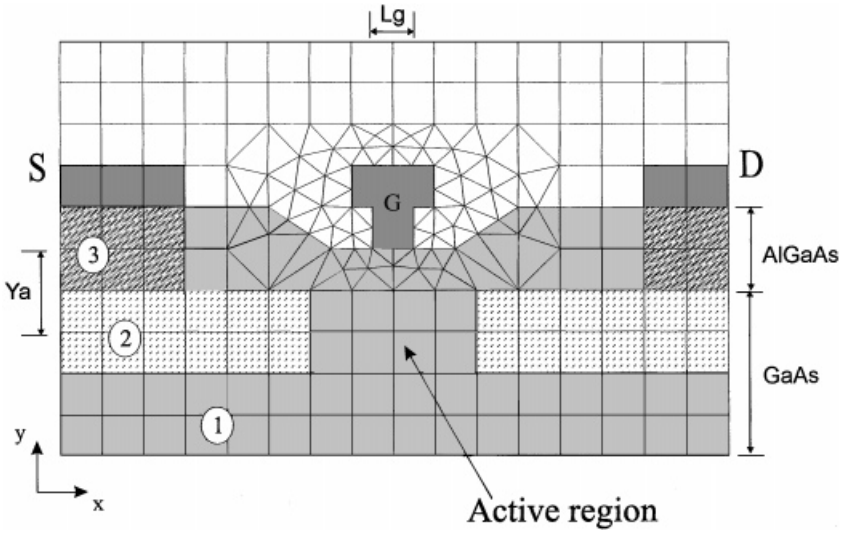

Figure 1. Cross-sectional view of the FET device under investigation. The mesh model is superimposed.

composed by the two gate-to-source and gate-to-drain currents, J_{GS} and J_{GD}, and by the channel current J_{ch}. A simple and efficient way to define these current contributions is to analytically relate them to the internal instantaneous voltages. In this way, the internal drain to source voltages can be viewed as the input parameters of the circuit model, while the gate-to-channel voltage represents the control parameter on which the dynamic parameters depend. The relation that defines the intrinsic equivalent circuit for the HEMT is

$$\mathbf{J}(\mathbf{r}, t) = J_{GS}\hat{y} + J_{GD}\hat{y} + J_{ch}\hat{x} = \frac{\partial}{\partial t}(C_{GS}V_{GS})\hat{y} + \frac{\partial}{\partial t}(C_{GD}V_{GD})\hat{y} + J_{DS}(V_{GD}, V_{DS}, x, t)\hat{x} \quad (2)$$

In Equation (2), $\hat{x}$ and $\hat{y}$ identify the unit vectors of the standard two-dimensional orthogonal reference frame (see Figure 1). The values of C_{GS} and C_{GD}, as well as that of $J_{DS}(V_{GD}, V_{DS}, x, t)$ are determined on the basis of the following analytical formulations:

$$C_{GS} = \frac{\varepsilon}{d}\left[L_G + \frac{\varepsilon_{GaAs}(V_{DS} + V_{SG} + V_{B0})}{qNY_A - qn_S}\right] \quad (3)$$

$$C_{GD} = \frac{\varepsilon_{GaAs}^2 L_G}{2dC_{GS} - 1.5\varepsilon_{GaAs}L_G} \quad (4)$$

where L_G is the gate length and n_S is the two-dimensional electron gas (2-DEG) density, whose expression is

$$n_S = \frac{-(\varepsilon/q)(V_{SG} + V_{B0}) + \varepsilon_{GaAs}NY_A^2/2\varepsilon_{AlGaAs}}{d} \quad (5)$$

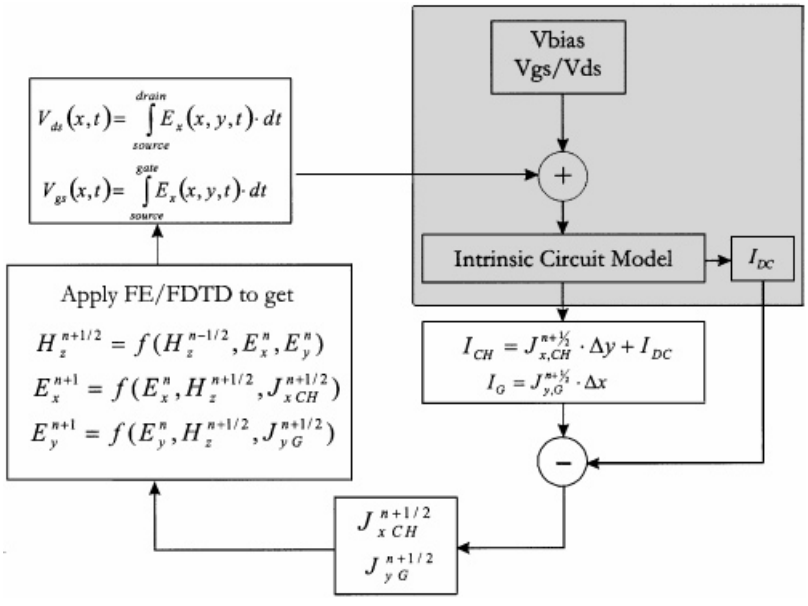

Figure 2. Flow chart of the global simulation scheme.

In Equation (5), the 2-DEG channel offset, d, is given by $d = 8 \times 10^{-9} + (\varepsilon_{GaAs}/\varepsilon_{AlGaAs}) Y_A$, Y_A and N being the AlGaAs layer thickness and doping, respectively. The permittivities ε_{AlGaAs}, ε_{GaAs} refer to the AlGaAs and GaAs regions, respectively. Finally, V_{B0} is the contact potential at the connection between the gate terminal and the AlGaAs semiconductor region. For the case under investigation, the following parameters values have been used: $N = 10^{18}$ cm^{-3}, $Y_A = 0.1$ μm, $L_G = 0.2$ μm, $V_{B0} = 0.8$ V.

The channel current density J_{DS} has been evaluated by curve fitting the DC data of the potential drop along the two regions below the source and drain contacts (regions 2 in Figure 1). The algebraic equation of the channel current is omitted here for brevity.

By following this procedure, the FET intrinsic behaviour is modelled in both the linear and pinch-off regions, where most of simulations have been performed. The current density derived from Equation (2) is then introduced into the numerical form of the Maxwell equations as required by a standard FD-TD scheme.

Conversely, the *extrinsic* part of the electron device exhibits geometrical and material inhomogeneities of complex shapes, so that the application of the more flexible hybrid FE/FD-TD method is needed. The two electromagnetic simulation schemes are interfaced by a suitable subgridding technique, without introducing an overlapping region between FD and FE. The features of the electromagnetic model are described in the next section.

A flowchart of the global simulation procedure is reported in Figure 2. The modelling algorithm starts by defining the bias voltages to be supplied to the device. They are introduced in the circuit model of the intrinsic region to provide the instant values of currents at the gate terminal and in the channel. The corresponding current densities are used as sources in the discretized Maxwell equations to obtain realistic estimates of the field distributions inside the

device. Then, these field distributions are integrated to determine a new set of input voltages for the circuit model. By updating these voltages, the new set of current densities at the following time step are determined through the use of the circuit model. The iterative procedure is in this way initialized.

3. FEATURES OF THE HYBRID ELECTROMAGNETIC TECHNIQUE

The general electromagnetic simulation procedure consists in a combination of FD-TD and FE-TD. It takes advantages of the features of both techniques. In particular, the FD method is used to analyse large regular homogeneous regions, and to account for the non-linear behaviour of the *intrinsic* region. Conversely, we resort to the FE to simulate localized irregular parts of the structure in the *extrinsic* zone of the device. Indeed, the FE method features greater flexibility and versatility than the FD-TD technique in modelling arbitrarily shaped regions, such as those encountered in the *extrinsic* part of GaAs FET devices (trapezoidal terminals, curved-doped regions). For instance, this allows us to analyse the actual geometry of the device with no 'staircasing' error. Moreover, by limiting the extent of the total FE region, a reduction of the resulting FE matrix size is obtained, which strongly increases numerical efficiency.

The interlacing between the EM fields in the structured and unstructured grids is performed according to the scheme presented in Reference [5]. In particular, the computational domain S is divided into two sub-domains S_{FD} and S_{FE}, corresponding to the FD-TD and FE regions, respectively, such that $S = S_{\mathrm{FD}} \cup S_{\mathrm{FE}}$. These two regions are next discretized using structured and triangular meshes, respectively, with common nodes shared at the interface but with no overlapping region ($S_{\mathrm{FD}} \cap S_{\mathrm{FE}} \varnothing$). The unstructured grid is confined to the vicinity of the irregular regions of the domain, and this allows us to limit the number of unknowns in the FE region to a moderate size.

The FD-TD solution in S_{FD} is conventional in nature and, hence, requires no further discussion. In S_{FE}, an FE formulation with curl-conforming vector edge basis functions is employed in the time domain to discretize the second-order vector wave equation. The resulting equations are solved by using an unconditionally stable procedure that makes use of a mixed backward and central difference scheme with two stability parameters Θ_1 and Θ_2 (see Reference [8]). In this operation, it is crucial to employ an unconditionally stable time domain formulation for the FE algorithm in problems with very small features that lead to large variations in the element size across the problem domain. This enables us to employ a time step which is identical to that dictated by the Courant condition in the FD-TD domain, where it is typically much larger than the corresponding one in the FE domain.

As far as the time-marching scheme adopted is concerned, let $\mathbf{H}_{\mathrm{BD}}^{n-1/2}$ be the magnetic field close to the interface between FD-TD and FE-TD regions in S_{FD}, at a generic time step t^n. Moreover, let $\mathbf{H}_{\mathrm{BE}}^{n-1/2}$ be the adjacent magnetic field located in the S_{FE} domain (see Figure 3). The electric field $\mathbf{E}_{\mathrm{B}}^{n}$ can be evaluated in accordance with the FD-TD algorithm, provided that the location of $\mathbf{H}_{\mathrm{BE}}^{n-1/2}$ coincides with that of the magnetic field in a fully-structured grid. To this end, we first identify the FE element which contains the node point location of the desired $\mathbf{H}_{\mathrm{BE}}^{n-1/2}$, and then evaluate it exactly from the knowledge of the electric fields in the element.

To complete the iterative procedure, all the electric fields $\mathbf{E}_{\mathrm{FD}}^{n}$ in the region S_{FD} are updated according to the FD-TD scheme, using the values of the magnetic fields $\mathbf{H}_{\mathrm{FD}}^{n-1/2}$ in the region S_{FD} together with the magnetic fields $\mathbf{H}_{\mathrm{BE}}^{n-1/2}$ at the interface. All of the magnetic fields $\mathbf{H}_{\mathrm{FD}}^{n+1/2}$ in

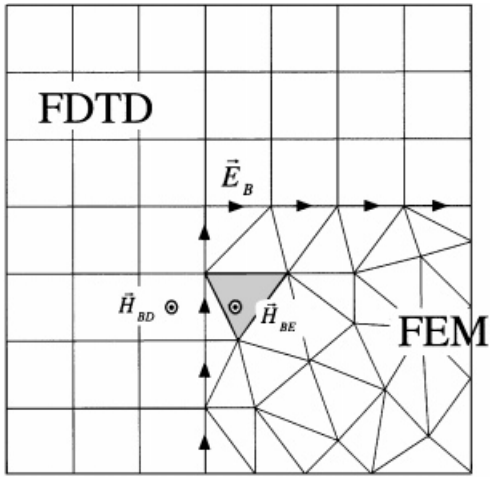

Figure 3. Treatment of the boundary conditions at the interface between the FD and FE regions.

the region S_{FD} can next be evaluated from $\mathbf{E}^n_{FD}$. The electric field $\mathbf{E}^n_B$ along the interface between S_{FD} and S_{FE} is used as a boundary condition (initial value in time, boundary value in space) for the FE procedure, so that the electric field $\mathbf{E}^n_{FE}$ at the time t^n can be evaluated throughout the region S_{FE}. The procedure can now be repeated to continue the time iteration.

As a final remark we underline that an interesting advantage of this hybrid method with respect to other techniques proposed in the literature is that it is formulated in such a way that no overlapping region is required between the FD region and the FE region [5]. Also, it is worth noting that, to obtain a higher degree of accuracy inside the *intrinsic* region the FD scheme should use cells in a nanometric scale. This can be attained by applying the subgridding technique proposed in Reference [7]. In particular, a finer FD discretization can be used around the intrinsic region, embedded in a triangular FE mesh which serves as a transition to an external coarser FD grid. This results in a discretization mesh that properly accounts for the different scale where propagation phenomena and charge transport phenomena take place. This aspect will be object of future work.

4. SIMULATION RESULTS

In order to show the basic characteristics of the model, a set of simulations are reported. We refer to the mesh model illustrated in Figure 1. The Gate region has been embedded in a triangular grid with 120 elements and solved by means of the FE-TD [9]. This allows us to take into account the correct shape of the bulk. The remaining part, which includes the Drain, the Source and the active channel, has been discretized according to a regular grid and solved by means of the FD-TD algorithm. The total FD-TD mesh is 25×50 square cells (0.1 μm cell size), and second-order absorbing boundary conditions (ABC) have been used at the top and bottom of the simulation region, while two perfectly magnetic conducting boundaries confine the numerical domain at the side walls. In the cross-sectional view of the same Figure 1, three different regions of the device

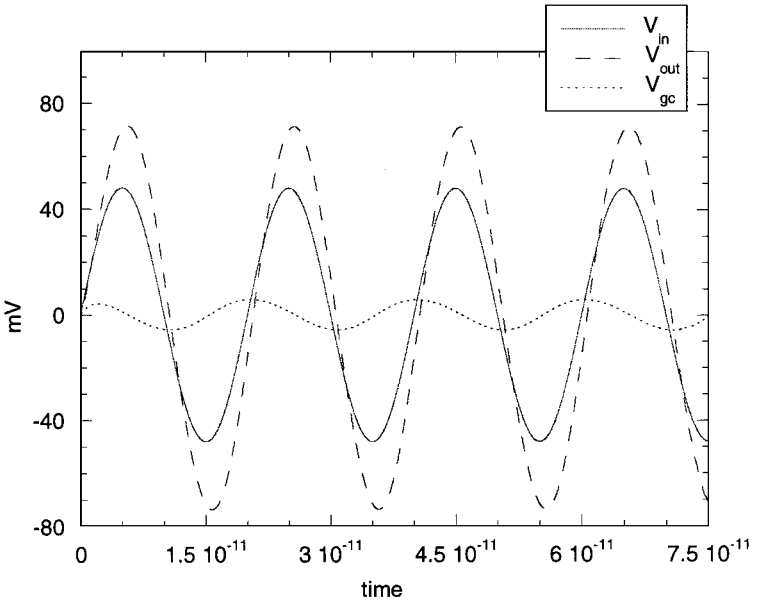

Figure 4. Output (dashed line) and control (dotted line) voltages as a function of time for a monochromatic input voltage (continuous line) at 50 GHz. Bias point: $V_{gs0} = -0.3$ V, $V_{ds0} = -1$ V.

can be identified with different electrical properties. In particular, region 1 (which comprises the channel) has electrical parameters equal to $\varepsilon_r = 13$, $\sigma = 0$ S/m; region 2 exhibits $\varepsilon_r = 13$, $\sigma = 200$ S/m, while region 3 is characterized by $\varepsilon_r = 13$, $\sigma = 2 \times 10^5$ S/m. The electrical contacts have been assumed to be perfect electric conductors. In all the simulations presented hereafter, the stability parameters Θ_1 and Θ_2 have been set to 0.3 and 0.4, respectively.

Different simulations have been performed considering either a harmonic dependence of the input voltage $V_{in} = V_{GS}$ or a wide-band (pulse) input voltage. In Figure 4 we show the output voltage $V_{out} = V_{DS}$ (dashed line) as a function of time for a monochromatic input voltage V_{GS} at 50 GHz (continuous line). In particular, the gate-to-channel voltage V_{GC} (dotted line), that controls the device transfer function, is also plotted. As can be seen from the same figure, the amplitude (peak value) of the input voltage is very small (about 50 mV) so that a small-signal analysis of the device can be performed. The bias point for V_{GS} and V_{DS} have been set to $V_{gs0} = -0.3$ V and $V_{ds0} = -1$ V, respectively. Figure 5 shows the same quantities but for a frequency of 75 GHz and for a different bias point of the gate-to-source DC voltage which has been set now to $V_{gs0} = -0.8$ V.

As well known from circuit analysis, if the amplitude (peak value) of the input voltage is increased and/or for values of the DC voltage V_{gs0} approaching -1 V, a non linear behaviour is encountered. This is shown in Figure 6, where the channel current I_{ch} is plotted vs. time for a peak value of the input voltage equal to 250 mV and for different bias points.

As a final result, we plot the input and output voltages as a function of time for a wide-band pulse. In particular, Figure 7 shows the behaviour of the output voltage (dashed line) when the input voltage (continuous line) is a wide-band-modulated pulse with modulation frequency of

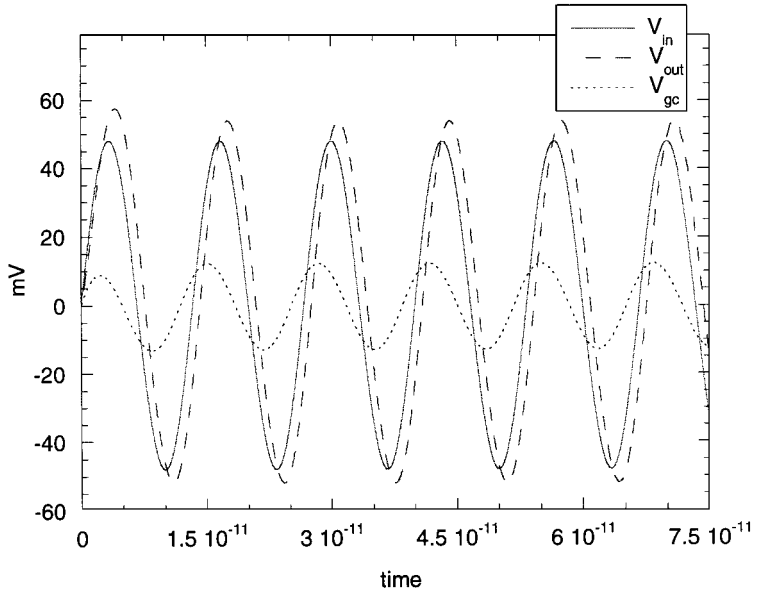

Figure 5. Output (dashed line) and control (dotted line) voltages as a function of time for a monochromatic input voltage (continuous line) at 75 GHz. Bias point: $V_{gs0} = -0.8$ V, $V_{ds0} = -1$ V.

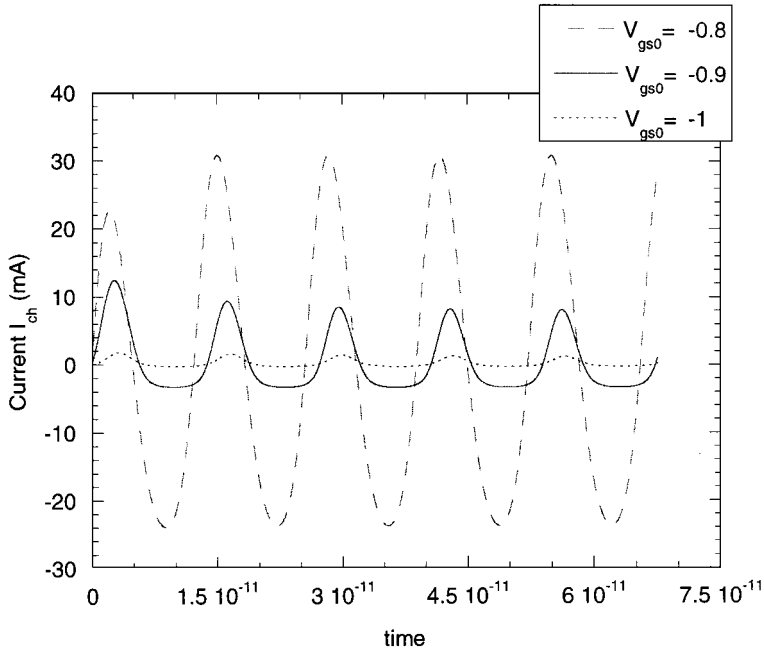

Figure 6. Channel current I_{ch} as a function of time for different values of V_{gs0} for a monochromatic excitation of 75 GHz.

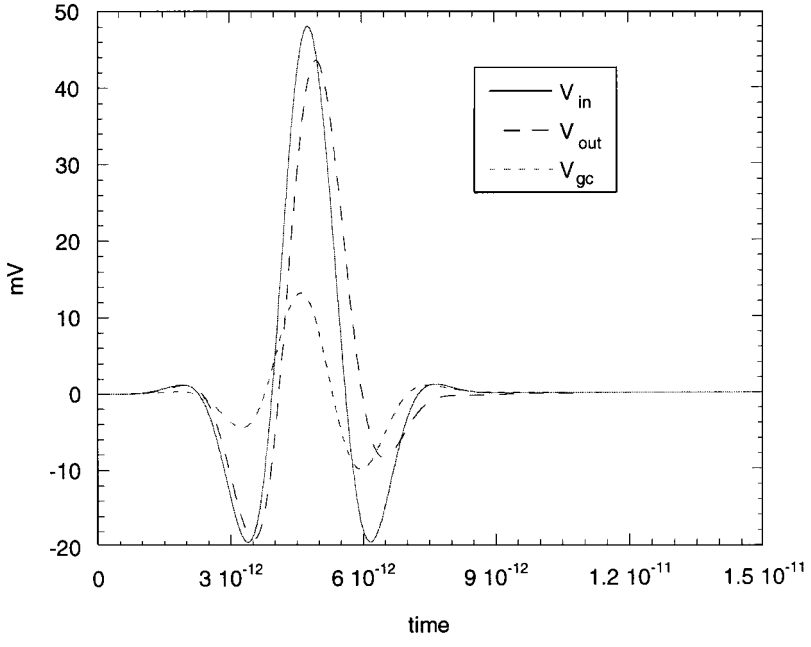

Figure 7. Output (dashed line) and control (dotted line) voltages as a function of time for a wide-band input voltage (continuous line). Bias point: $V_{gs0} = -0.5$ V, $V_{ds0} = -1$ V.

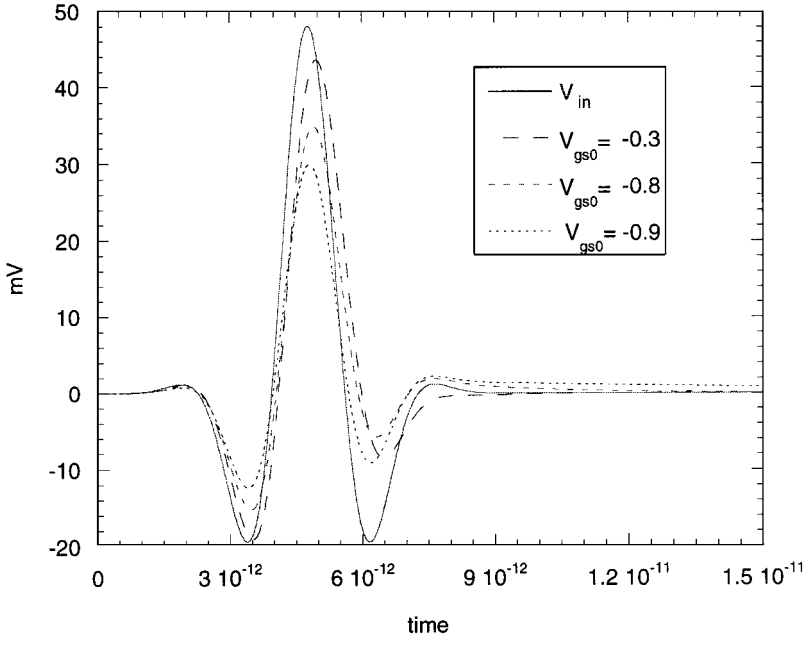

Figure 8. Output voltage for different values of V_{gs0}. The input voltage (continuous line) is shown as reference.

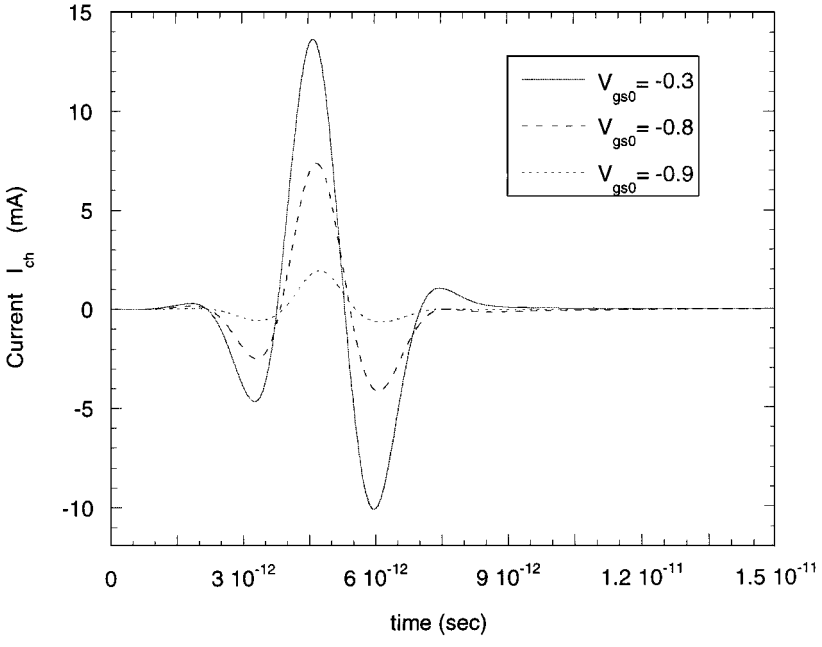

Figure 9. Channel current I_{ch} as a function of time for different values of V_{gs0}.

300 GHz and a band of 200 GHz. The bias point has been set to $V_{gs0} = -0.5$ V and $V_{ds0} = -1$ V, respectively. The gate-to-channel voltage (control voltage) is shown (dotted line) in the same figure. The output voltage for different DC voltages V_{gs0} is reported in Figure 8. A variation both in amplitude and in phase can be observed. The channel currents I_{ch} for the same DC voltages V_{gs0} are plotted in Figure 9. By Fourier transforming the input and output voltages, the device transfer function (voltage gain) can be obtained; it is shown in Figure 10(a) (module) and 10(b) (phase). Different bias points for the DC voltage V_{gs0} have been considered. As can be seen from both figures, the device voltage gain collapses to low values, losing at the same time its linear properties for values V_{gs0} less than -0.7 V.

5. CONCLUSIONS

A hybrid FD/FE method, directly working in time domain, has been applied to analyse high-frequency FET structures. In particular, a set of simulations has been carried out considering a cross section of a AlGaAs\GaAs HEMT as a test bench. This hybrid approach has revealed very efficient from a numerical point of view with respect to a simulation procedure completely based on the FD method; moreover, it exhibits a higher flexibility to match complex geometrical and material configurations. A set of numerical results has been shown to demonstrate the effectiveness of the simulation technique.

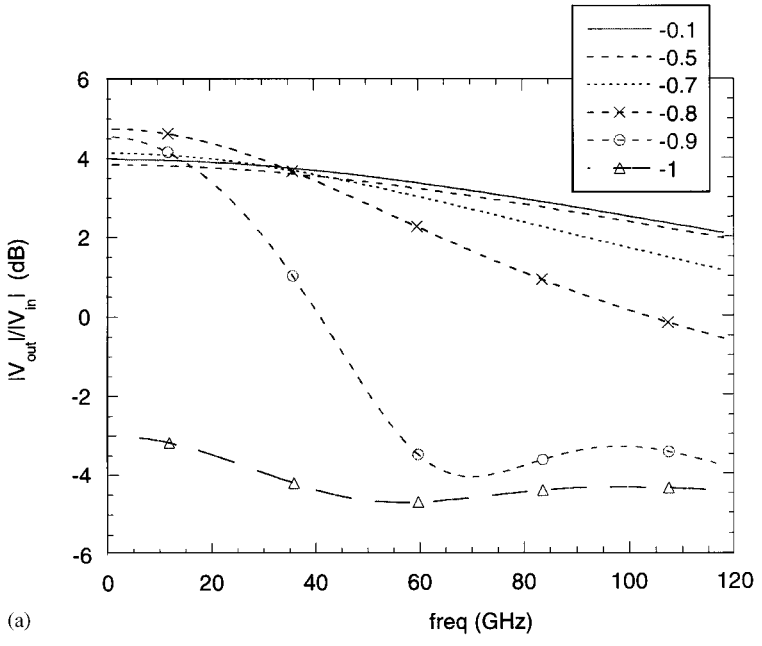

(a)

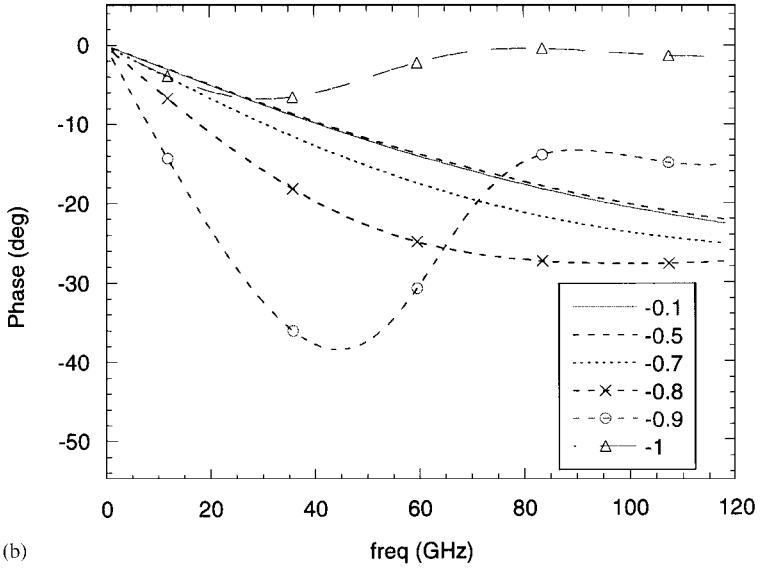

(b)

Figure 10. Module (a) and phase (b) of the voltage transfer function versus frequency for different values of V_{gs0} ($V_{ds0} = -1$ V).

REFERENCES

1. Alsunaidi MA, Imtiaz SM, El-Ghazaly SM. Electromagnetic wave effects on microwave transistor using a full-wave time-domain model. *IEEE Transactions Microwave Theory Techniques* 1996; **MTT-44**(6):799–808.
2. Cidronali A, Collodi G, Leuzzi G, Manes G. Numerical analysis of a 0.2 μm AlGaAs\GaAs HEMT including electromagnetic effects. *IEEE International Symposium on Compound Semiconductor*, San Diego, CA, U.S.A., 7–11 September 1997.
3. Heinrich W, Hartnagel HL. Wave propagation on MESFET electrodes and its influence on transistor gain. *IEEE Transactions on Microwave Theory Techniques* 1997; **MTT-35**(1):1–8.
4. Wu R-B, Itoh T. Hybrid finite-difference time-domain modeling of curved surfaces using tetrahedral edge elements. *IEEE Transaction on Antennas and Propagation* 1997; **AP-45**(8):1302–1309.
5. Monorchio A, Mittra R. A hybrid finite element/finite difference time domain (FE/FD-TD) technique for solving complex electromagnetic problems. *IEEE Microwave and Guided Wave Letters* 1998; **8**(2):93–95.
6. Selleri S, Dauvignac JY, Pelosi G, Pichot Ch. Comparison between FD-TD and hybrid FDTD-FETD as applied to scattering and antenna problems. *Microwave and Optical Technology Letters* 1998; **18**(4):247–250.
7. Monorchio A, Mittra R. A novel subgridding scheme based on a combination of the finite element and finite difference time domain methods. *IEEE Transactions on Antennas and Propagation* 1998; **AP-46**(9):1391–1393.
8. Lee J-F, Lee R, Cangellaris A. Time-domain finite-element methods. *IEEE Transactions on Antennas Propagation* 1997; **45**(3):430–441.
9. Pelosi G, Coccioli R, Selleri S. *Quick Finite Elements for Electromagnetic Waves*. Artech House Publ.: London, 1998.

